AAPM REPORT NO. 52

Quantitation of SPECT Performance

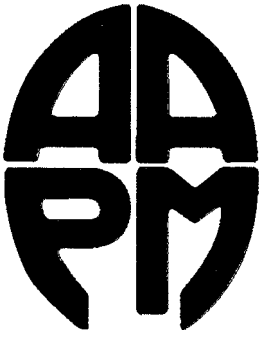

Published for the
American Association of Physicists in Medicine
by the American Institute of Physics

AAPM REPORT NO. 52

Quantitation of SPECT Performance

REPORT OF AAPM NUCLEAR
MEDICINE COMMITTEE TASK GROUP 4

Members

L. Stephen Graham
Frederic H. Fahey
Mark T. Madsen
Andries van Aswegen
Michael V. Yester

Reprinted from MEDICAL PHYSICS, Vol. 22, Issue 4, April 1995

April 1995

Published for the
American Association of Physicists in Medicine
by the American Institute of Physics

Further copies of this report ($10 prepaid) may be obtained from:

American Association of Physicists in Medicine
American Center for Physics
One Physics Ellipse
College Park, MD 20740-3843

(301) 209-3350

International Standard Book Number: l-56396-485-6
lnternational Standard Serial Number: 0271-7344

Published by the American Institute of Physics
500 Sunnyside Blvd., Woodbury, NY 11797-2999

Printed in the United States of America

Quantitation of SPECT performance: Report of Task Group 4, Nuclear Medicine Committee

L. Stephen Graham (Task Group Chairman), Frederic H. Fahey, Mark T. Madsen, Andries van Aswegen, and -Michael V. Yester

(Received 17 March 1994; accepted for publication 7 November 1994)

A comprehensive performance testing program is an essential ingredient of high-quality single-photon emission computed tomography (SPECT). Many of the procedures previously published are complicated, time consuming, or require a special testing environment. This Task Group developed a protocol for evaluating SPECT imaging systems that was simple, practical, required minimal test equipment, and could be performed in a few hours using processing software available on all nuclear medicine computers. It was designed to test rotational stability of uniformity and sensitivity, tomographic spatial resolution, uniformity and contrast, and the accuracy of attenuation correction. It can be performed in less than three hours and requires only a Co-57 flood source, a line source, and a tomographic cylindrical phantom. The protocol was used 51 times on 42 different cameras (seven vendors) by four different individuals. The results were used to establish acceptable ranges for the measured parameters. The variation between vendors was relatively small and appeared to reflect slight differences in basic camera performance, collimation, and reconstruction software. Individuals can use the tabulated values to evaluate the performance of individual systems.

I. INTRODUCTION

The use of single-photon emission tomography has become widespread since its introduction in the late 1970s. SPECT has been especially useful in providing tomographic images of myocardial perfusion, the lumbar spine, and cerebral perfusion. Much of the research involving radiolabeled antibodies has been performed on SPECT instrumentation. SPECT provides high-contrast images of the three-dimensional distribution of internally distributed radiopharmaceuticals.[1-6] These images not only allow accurate anatomic localization of abnormalities, but also have the potential for providing quantitative information about both the regional concentration of radioactivity and its volume of distribution. However. the acquisition of high-quality SPECT images requires careful attention to detail and the routine performance of quality control procedures to avoid the production of artifacts.[7,8]

Quality control procedures and methodology for acceptance testing of SPECT systems have been published. These include the NEMA standards[9] and AAPM report #22.[10] Although these reports are quite comprehensive, they suffer from two major deficiencies. First, many of the tests described require special equipment and sophisticated software and cannot be completed within a reasonable time frame. Second, there is no range of acceptable values given for the tests.

The goal of this Task Group was to describe a set of quality control tests and present typical results that can be used to provide confidence that a SPECT system is in proper working order. In this sense, the tests need only be comprehensive enough to detect a problem. When problems are detected, more rigorous testing and a call to field service may be warranted.

The protocols presented in this report were designed with the following features in mind:

(1) the key performance parameters of rotational uniformity and sensitivity, tomographic spatial resolution, uniformity and contrast, and the accuracy of attenuation correction must be tested;
(2) the set of tests can be completed within three hours by a qualified and experienced medical physicist, or under his/her direct supervision;
(3) the protocols do not require special analysis software; and
(4) the tests must conform as much as possible to the standard SPECT tests described in AAPM report #22.[10]

II. BACKGROUND INFORMATION

A. Rotational uniformity

Photomultiplier tubes (PMT) are known to undergo gain shifts when their spatial orientation changes with respect to an external magnetic field.[11,12] These effects can be produced by the earth's magnetic field (»0.05 mT) as well as fields around magnetic resonance imaging systems and particle accelerators such as cyclotrons. Maximum gain shifts occur when the tube is rotated through 90° between the azimuthal and orthogonal directions relative to the external field. A 1% change in the secondary emission ratio per dynode results in a change of more than 10% in the charge gain of a tube. Consequently, detector assemblies with inadequate magnetic shielding can experience gain shifts sufficient to cause significant angle-dependent spatial nonuniformities, some appearing in the shape of a half-moon.[13-15] Changes in the observed count rate as a function of angle can also be produced.

Manufacturers have incorporated magnetic shielding into SPECT detector assemblies to minimize PMT gain shifts. The smaller tubes used in current generation systems are easier to shield against external magnetic fields than larger ones.[16]

State-of-the-art SPECT systems should not exhibit significant angular-dependent nonuniformities if strong magnetic fields are not present in the environs.

Work by Johnson et al. indicates that nonlinearities as a function of angle may also be caused by thermal gradients in the detector housing.[17] These nonlinearities in turn produce changes in uniformity which can generate artifacts.

 0094-2405/95/22(4)/401/9/$6.00

B. Spatial resolution

Because of the importance of spatial resolution in SPECT studies[18,19] it is essential to periodically verify that there has been no deterioration in this parameter. Spatial resolution is commonly quantified from the full-width-at-half-maximum (FWHM) of the line spread response function. In planar imaging it depends on the intrinsic capabilities of the scintillation camera, the geometrical properties of the collimator, and the presence of scatter. In SPECT, additional factors affect resolution because the information is gathered over multiple angles. Precise positioning of the gantry, detector, and table and calibration of the center of rotation (COR) is required. In addition, the reconstruction matrix size, filter, and use of pre- and post-processing procedures can affect the measured spatial resolution."

Line spread functions measured from reconstructed images of line sources include the effects of all the factors. If a Ramp filter is used, the measured FWHM of the line spread function should be essentially the same as the value obtained for a planar view (or slightly worse) at a distance equal to the average radius of rotation (ROR). Therefore. the SPECT/planar ratio of the FWHMs is a sensitive indicator of spatial resolution degradation associated with malfunctions in the SPECT system.

C. Tomographic uniformity

The uniformity of reconstructed images is very sensitive to scintillation camera field uniformity. There are two primary causes of field nonuniformities in flood field images from Anger scintillation cameras.[20,22] Approximately one-third of the nonuniformity is caused is caused by energy-axis shifts of the photopeak at different points in the field of view [20,21,23] The remaining two-thirds is primarily due to spatial nonlinearities (distortion). All state-of-the-art Anger cameras incorporate on-the-fly energy and linearity correction circuitry. However, energy and linearity correction alone may not be adequate for some tomographic studies because uniformity requirements are considerably more stringent and in many systems the correction circuits do not correct for collimator nonuniformities. [7]

Spatial nonuniformities in the scintillation camera response and collimator defects can produce count losses or excesses in the same location on each of the acquired projection images. For circular detector orbits, these manifest themselves as concentric ring or "bull's eye artifacts and even more complicated artifacts for noncircular orbits. [15,24] Nonuniformities which are inconsequential in planar images can produce artifacts in SPECT reconstruction\ that make the images unreadable.'" The intensity of the artifact depends upon the magnitude of the nonuniformity. its location with respect to the axis of rotation, and the size of the object.[14,25]

Because the level of uniformity required for artifact-free SPECT images is typically lower (more stringent) than that inherent in many scintillation cameras, the projection data may need to be corrected for nonuniformities.[20,26,27] The most common approach is to acquire a high-count flood, generate a correction matrix, and then apply a multiplicative correction. It has been reported that the projection images must be corrected to within ± 1% integral uniformity in order to generate artifact-free SPECT images and that this requires a 30 million count flood (»10 000 counts/pixel in 64X64 matrix) to be acquired for the correction matrix.[14] Although a lower count flood may be adequate to correct low-frequency nonuniformities (that may be caused by improperly tuned phototubes, for example) 30M counts are actually necessary to ensure that the statistical fluctuations in the correction matrix do not themselves lead to artifacts.

For some state-of-the-art SPECT cameras with excellent uniformity and stable electronics, it may not be necessary to apply uniformity correction. However, most older SPECT systems require uniformity correction. This being the case, the following caveats should be observed.

Floods must be collected with the same collimator, zoom, and matrix size (not required by some vendors) that is used for clinical studies. In addition, the acquisition count rates should not exceed 20K-30K cps.28 Because the uniformity of many scintillation cameras is energy dependent, Tc-99m-based correction matrices may not be appropriate for clinical studies that utilize other radionuclides. When fillable flood phantoms are used, extreme care must be taken to be sure that they are thoroughly mixed, the sides are flat, and bubbles are not present.[8,14] Even though Co-57 sheet sources have less scatter than liquid-filled floods, they are satisfactory for clinical studies.[26]

Finally, one important fact must be kept in mind. Flood field correction should not be used to compensate for cameras operating at less than peak performance or with serious collimator damage. It is preferable to identify these problems and correct them.

D. System performance

The existence of a current COR calibration and high-count flood does not guarantee optimum operation of a SPECT system. Changes in analyzer window size and a loss of energy resolution will produce a loss in image quality that will not be evident from any of the tests that have been described so far.

Several phantoms can be used to evaluate overall SPECT system performance. These include the Data Spectrum Corporation "Jaszczak" phantom and the Nuclear Associates "Carlson" phantom. Both are commercially available and can be used to evaluate reconstruction noise, check for artifacts, determine the accuracy of field uniformity and attenuation corrections, and measure contrast.[27] In addition, they can be used to evaluate the effect of using different collimators, filters, acquisition times, noncircular orbits, 180° vs 360° acquisitions, etc.[29,30]

III. METHODS

In the protocols that follow, it will be assumed that all the routine calibrations and daily or weekly QC procedures (floods and resolution tests) have been performed on the SPECT system. In addition, it will be assumed that the center-of-rotation calibration, the pixel size calibration, and the high-count uniformity correction matrix are current.

A. Protocols

The following protocols are to be used for collecting and analyzing the data. A worksheet is provided in Appendix A to facilitate data handling.

1. Rotational field uniformity and sensitivity

The method used to assess magnetic field effects and thermal gradients on uniformity is similar to that recommended by NEMA.[9] A Co-57 flood source (larger than the UFOV) is securely fastened to the collimator and the following procedure is used:

(1) Set a 20% symmetric analyzer window.

(2) Collect a 5 million count 64X64-image with the detector at 0°.

(3) Repeat for 90°, 180°, 270°, and 360° using the time required to collect the 5 million count image at 0°.

(4) Calculate the maximum sensitivity variation:

$$\text{Max Sens Var}(\%)=\pm\frac{\text{Max tot cts-Min tot cts}}{\text{Max tot cts+Min tot cts}}\times 100.$$

(5) Subtract the 0° flood image from the flood images collected at 90°, 180°, 270°, and 360°.

(6) Subtract the 270° image from the 90° image.

Analysis: Check each of the difference images for structured, nonrandom patterns. File for future reference. The Maximum Sensitivity Variation should not exceed 0.75%

2. Spatial resolution

The protocol presented here is a variation of that suggested in the 1986 edition of NEMA Performance Measurements of Scintillation Cameras. Section 4.4.3[9] and AAPM Report #23.[10] The line source used for this measurement consists of a fillable tube at least 30 cm in length with an inside diameter of less than 2 mm. Such sources are commercially available (Nuclear Associates, Carle Place, NY) or can be fabricated from catheter tubing taped to a rigid piece of cardboard.

(1) Fill the central line source with Tc-99m at a concentration of at least 37 TBq/m^3 (1ø mCi/cm^3). All the mea'-surements are made in air with no additional scattering material.

(2) Mount the phantom on the end of the table, or the frame to which the table connects, so that the source is suspended over the camera with minimal interference from the pallet or other objects.

(3) Set the radius of rotation to 20 cm as measured from the collimator face. If this is not possible, use the smallest that can otherwise be obtained.

(4) Adjust the table so the line source is as close as possible to the axis-of-rotation and adjust the phantom so it is parallel to the axis-of-rotation (both the detector and phantom must be level).

(5) Set the acquisition matrix to 128×128 and the number of views to 128 (120) views over 360°.

(6) If necessary, use an image magnification factor (zoom) that will give a pixel size in the range of 3.0-3.5 mm.

(7) Acquire the data set using a time that will give at least 100k counts for the first projection.

TABLE I. Reconstruction filters and cutoff values for SPECT (measurements of spatial resolution involving line sources).

Computer	Filter name	Cutoff
ADAC 3300/33000	Butterworth	0.95 Nyquist
ADAC Pegasys	Ramp	1 Nyquist
Elscint	Ramp	1 Nyquist
General Electric	Ramp	1.56/cm[a]
Picker PSC512	Filter 0	
Picker Prism	Ramp	0.5/pixel
Siemens MaxDelta	Ramp	1 Nyquist
Sophy	"None"	
Summit Spectrum	Ramp	1 Nyquist
Toshiba	Ramp	1 Nyquist
Trionix	Ramp	1 Nyquist

[a]Cutoff calculated for pixel size of 0.32 cm. For other pixel sizes, the cutoff must be calculated as described in the vendor's procedure manual.

(8) Use a Ramp filter to reconstruct a 10-mm transverse section (or add three sections together) near the top of the line. Field uniformity and attenuation correction need not be applied. Refer to Table I for assistance in selecting filter values for a number of different computer systems.

(9) Draw a l-pixel-wide profile in the X direction through the hottest pixel in the reconstructed image and calculate the FWHM by linear interpolation. (The maximum error in the use of linear interpolation as opposed to Gaussian fitting is less than 5%. Therefore, a Gaussian fit does not need to be done.)

(10) Repeat step 9 in the Y dimension.

(11) Repeat steps 8-10 for a section near the bottom of the line.

(13) Acquire a 500k count planar image of the line phantom at the same average distance as the radius-of-rotation (20 cm).

(13) Calculate FWHMs of lo-mm-wide (3 pixels) count profiles for the planar image at approximately the same positions on the line as for the reconstructed slices.

(14) Calculate the SPECT/planar ratio for the top and bottom of the line.

Analysis: The SPECT/planar ratio should not exceed 1.1. If it does, a new center-of-rotation calibration should be performed and the test repeated. A significant difference (greater than 20%) in the FWHM between the top and bottom of the line may mean that the electronic axis of the camera is rotated.

3. System performance: Tomographic uniformity and contrast

For system performance the Task Group chose to use a Data Spectrum Corporation "Jaszczak" SPECT phantom filled with 300-370 MBq (8-10 mCi) of a uniformly mixed solution of Tc-99m. Data were collected with the following protocol:

(1) Mount a general purpose collimator. If a high-resolution collimator is used, the total activity can be increased to approximately 555 MBq (15 mCi).

TABLE II. Reconstruction filters and cutoff values for SPECT (measurements of integral uniformity, rms noise, and contrast).

Computer	Filter name	cutoff
ADAC 3300/33000	Hamming	1 Nyquist
ADAC Pegasys	Hann	1 Nyquist
Elscint	Hann	Parameter a =0 Parameter b = 1 Parameter c = 1
General Electric	Hann	0.76/cm[a]
Picker PCS512	Filter 3	
Picker Prism	Hann	0.5/pixel
Siemens MaxDelta	Shepp-Logan/Harm	1 Nyquist
Sophy	Hann	1 Nyquist
Summit Spectrum	Hann	1 Nyquist
Toshiba	Hann	1 Nyquist
Trionix	Hann	1 Nyquist

"Cutoff calculated for pixel size of 0.64 cm. For other pixel sizes, the cutoff must be calculated as described in the vendor's procedure manual.

(2) Position the phantom on the end of the SPECT table with the central axis of the phantom parallel to, and as close as possible to, the axis-of-rotation. Fasten it securely in place. (Note-some SPECT tables have metal plates near the end and one should avoid locating the phantom on top of these plates.)
(3) Set the average radius-of-rotation to 20 cm or the smallest that can otherwise be obtained.
(4) Set a symmetrical analyzer window to 20% and determine the time needed to collect 500k counts for the first projection.
(5) Set the acquisition matrix to 64X64 and the number of views to 64 (60) views over 360°.
(6) If necessary, use an image magnification factor (zoom) that will give a pixel size in the range of 6.0-7.0 mm.
(7) Acquire the SPECT study.
(8) Reconstruct the data without system flood correction (if possible) using a Hann filter and a one Nyquist cutoff. See Table II for assistance in selecting the reconstruction parameters for systems that do not offer this filter and cutoff selection directly.

TABLE III. Number of samples by vendor and model.

Model	Number of times used for samples
ADAC Genesys	4
Elscint 409AG	3
Elscint 415-1	1
Elscint SP-6	1
GE 400 AC/T	8
GE 3000 XR/T	1
Picker SX-300	1
Siemens ZLC/Orbiter	13
Siemens Diacam	3
Siemens Rota Camera	2
Sophy DS7	2
Sophy DSX	4
Toshiba GCA-90lA/SA	6
Toshiba GCA-602A/SA	2
Total=51	

TABLE IV. Loss of spatial resolution in tomography.

	Ratio of SPECT to Planar			
Profile location	<l.049	1.05-1.099	1.1-1.149	>1.15
Top horizontal	26	8	6	3
Top vertical	26	9	2	5
Bottom horizontal	24	9	2	3
Bottom vertical	24	7	4	3
Total	100	33	14	14
Percent of Total	62.1%	20.5%	8.7%	8.7%

(9) Apply attenuation correction using a linear attenuation coefficient of 0.ll/cm or the default value (some systems require slightly different coefficients).
(10) Repeat steps 8 and 9 with flood correction applied.

Analysis-Attenuation correction:

(1) Select a transverse section from a uniform part of the phantom (no cold spheres or rods visualized).
(2) Draw a 5-pixel-wide horizontal count profile across the center of the phantom and verify that it is flat.
(3) Repeat step 2 in the vertical direction.
(4) If the image is over- or undercorrected for attenuation, check to see that the pixel size calibration is correct. If it is not, do a pixel size calibration. If it is, modify the attenuation coefficient appropriately and repeat the reconstruction. A profile that is linear but which has a large nonzero slope indicates that the boundary selected for attenuation correction is incorrect or that a software error is present. However, with a coarse matrix such as 64 X64, it is often impossible to get perfectly symmetric boundaries.

Analysis-Image uniformity and root-mean-square (rms) noise:

(1) Display the entire set of reconstructed images that has not been flood corrected and examine each image for the presence of artifacts. Minor artifacts may be present at the high-count density used in this study but profound ring artifacts should not be present.

(2) Select one or more uniform slices and draw a 15 X 15-pixel square region-of-interest (ROI) centered on the image(s) (60X60 ROIs must be used for ADAC 3300 and 33000 systems).

TABLE V. Measured integral uniformity[a] and root-mean-square (rms) for Jaszczak phantom images.

	Integral uniformity (%)	rms noise (%)
Without flood correction (n =31)		
Average±l σ	14.11±4.2	5.07±0.614
Percent standard deviation	29.5	12.1
Range	10.44-29.0	4.18-6.09
With flood correction (n =26)		
Average ±l σ	14.73±4.07	5.41±1.76
Percent standard deviation	27.6	32.6
Range	6.92-23.8	2.74-9.00

[a]See text for definition.

(3) Record the mean counts per pixel, the maximum and minimum pixel counts within the ROI, and the standard deviation, if provided. If the maximum and minimum pixel counts of the ROI are not output, use single-pixel ROIs to get the values.

(4) Calculate the reconstructed image integral uniformity by the following equation:

$$\text{integral uniformity}(\%) = \frac{(\text{maximum pixel ct} - \text{minimum pixel ct})}{(\text{maximum pixel ct} + \text{minimum pixel ct})} \times 100.$$

(5) Calculate the rms noise:

$$\text{rms noise}(\%) = \frac{\text{standard deviation}}{\text{mean pixel value}} \times 100.$$

(6) Apply flood correction and repeat all steps using matched slices(s).

(7) Acceptable values should fall within the following ranges:

Without flood correction:

integral uniformity: 9.90%-18.3%

rms noise: 4.5%-5.7%

With flood correction:

Integral uniformity: 10.7%-18.8%

rms noise: 3.6%-7.2%.

Comment: It is not unusual for the flood corrected image(s) to have higher integral uniformity and rms noise values. Some systems produce results that consistently fall at the top, or bottom, of the ranges, depending on the characteristics of the "general purpose" collimator, the precise definition of the reconstruction filter, and the specific characteristics of the reconstruction software.

Analysis-Contrast:

(1) Display the entire data set and select the transverse section where the cold spheres are most clearly defined. Note the number of spheres that can be visualized.

(2) For each sphere in the chosen slice, determine the number of counts in the "coolest" pixel.

(3) Calculate the contrast for the largest sphere.

$$\text{contrast} = \frac{(\text{average pixel cts from uniform section} - \text{min pixel cts})}{\text{average pixel cts from uniform section}}$$

(4) Repeat step 3 for all spheres visualized.

(5) Repeat all steps for the flood-corrected data set.

(6) Acceptable values should fall within the following ranges for general purpose collimators with flood correction applied:

Sphere size (mm)	Minimum	Maximum
31.8	0.53	0.73
25.4	0.35	0.56
19.1	0.21	0.38
15.4	0.11	0.27

Comment: As with integral uniformity and rms noise values, some systems will produce results that consistently fall at the top, or bottom, of the ranges because of differences in collimator, filter design, and reconstruction software. Also, head tilt, gantry flexing, and tilt of the phantom relative to the axis-of-rotation will produce a loss of contrast.

B. Precision of measurements

To evaluate the precision of integral uniformity and root-mean-square measurements, seven consecutive Jaszczak phantom studies were performed on one SPECT system. After each study, the imaging time for the subsequent study was increased to compensate for radionuclide decay so that each data set contained essentially the same total number of counts. No other changes were made between acquisitions. The individual acquisitions were reconstructed and analyzed as described.

A review of the complete data set indicated that for three vendors, data had been collected on six different cameras of the same model. These were analyzed to provide information about variations in setup techniques and positioning, as well as the effect of variations in implementation of the "same" filter on different computers.

IV. RESULTS

In this series, 51 performance tests were performed on 42 different SPECT systems. With respect to intrinsic uniformity, satisfactory operation of the cameras included in this study was determined by a review of acceptance test measurements or routine quality control results done prior to data collection. In all but one known case, center-of-rotation calibrations were done within 4 days of the time the SPECT studies were acquired. The distribution of cameras is shown in Table III. No results are included for any multiple-head SPECT system used as such.

A. Angular uniformity and sensitivity

Sensitivity as a function of angle was measured with Co-57 floods on 23 cameras. The values ranged from 0.06%-1.3% and had an average of 0.33%. Only one camera showed a variation in uniformity as a function of angle. This was due to movement of the collimator within the detector housing during rotation.

TABLE VI. Measured contrast in Jaszczak phantom images without flood correction (sample size=32).

Sphere size (mm)	31.8	25.4	19.1	15.4
Average contrast $\pm 1\sigma$	0.635±0.093	0.445±0.090	0.284±0.086	0.191±0.075
Percent standard deviation	14.6	20.2	30.3	39.3
Range of values	0.421–0.790	0.308–0.690	0.128–0.560	0.026–0.370

TABLE VII. Measured contrast for flood corrected Jaszczak phantom images (sample size=30).

Sphere size (mm)	31.8	25.4	19.1	15.4
Average contrast $\pm 1\sigma$	0.628±0.097	0.454±0.103	0.294±0.085	0.193±0.080
Percent standard deviation	15.4	22.7	28.9	41.4
Range of values	0.429–0.780	0.271–0.680	0.150–0.540	0.026–0.342

B. Spatial resolution

As measured by the FWHM, 62% of the individual measurements showed a loss of spatial resolution of less than 5% relative to planar measurements (Table IV). A total of 83% had a loss of less than 10%. the value which was considered acceptable given the errors associated with this measurement.

C. Uniformity

Measurements of integral uniformity (IU) and rms noise showed a wide variation (Table V). The application of flood correction did not produce a significant change in the mean values but both IU and rms noise increased (poorer uniformity, more noise).

D. Contrast

The results of the contrast measurements are shown in Tables VI and VII. Contrast decreased with decreasing sphere diameter, as would be expected. It is important to note that the percent standard deviation of the measured values increased markedly with decreasing sphere size whether or not flood correction was applied.

E. Precision

The average IU and rms noise measurements for the camera used in the study of precision were higher than for the average of all SPECT systems in the database (Table V vs Table VIII). However, the percent standard deviations for the IU and rms noise were approximately one-third and one-half, respectively, those obtained for the database as a whole.

Similar results were seen in the contrast measurements (Tables VI, VII, and IX). For the 31.8- and 25.4-mm spheres, the measured contrast in the study of precision was approximately 20% higher than those of the entire database. However, there was no significant change in contrast for the 19.1- and 15.4-mm spheres. As would be expected. the percent standard deviations were much smaller than for the complete database.

Data for the same model cameras located at different hospitals cannot be directly compared with the values shown in Tables VIII and IX because different computers and reconstruction algorithms were used. However, it can be stated that the increase in percent standard deviation of the IU and rms noise values was not as large as those of the database as a whole (Table V). The same was true for the contrast values (Table VII).

TABLE VIII. Precision of integral uniformity and root-mean-square (rms) noise measurements for Jaszczak phantom images (N=7).

	Integral uniformity	rms noise
Without flood correction		
Average $\pm 1\sigma$	20.00±1.91	7.37±0.627
Percent standard deviation	8.84	6.82
Range	17.80–22.59	6.82–9.861

V. DISCUSSION

Despite the relatively large number of cameras included in the database, the sample size for each model, or even each vendor, was still quite small (Table III). However, if the protocol was carefully followed and the performance is deemed acceptable based on the values presented in the "Analysis" section, then the camera is performing satisfactorily.

As can be seen from Table IV, 17% of the cameras showed a loss of spatial resolution in SPECT of more than 10%. In most cases this was caused by improper center-of-rotation (COR) correction.[27,28,31,32] The problem was eliminated by a new COR calibration. Because use of a filter other than the Ramp will produce an increase in the FWHM, it is essential that the filters presented in Table I be used. An apparent loss or gain of spatial resolution can be caused by failure to position the phantom properly so that the distance for the planar image is the same as the average radius-of-rotation. If the line source is more than 10 cm from the axis-of-rotation, the difference between the measured radial and tangential FWHM will be significantly more than 10%.[9]

It should also be noted that all vendors do not define the Ramp filter in the same way. The proper Ramp filter for discrete data has a spatial kernel defined by f(n) = ¼ for n =0, $f(n)=1/(n^2p^2)$ for odd values of n and $f(n)=0$ for even values of n .[33] When a true Ramp function is used, the reconstructed image has a negative dc offset which artificially sharpens the contrast and can also affect the FWHM. In such systems it is possible to obtain a FWHM ratio less than 1. Variations in the handling of negative numbers in the reconstructed image can produce a similar effect.

High values of integral uniformity (IU) and/or root-mean-square noise (rms noise) in the Jaszczak phantom study are generally caused by uncorrected nonuniformities in the detector or collimator. Such findings could also be caused by inadequate mixing of the Tc-99m in the Jaszczak phantom or in the flood field phantom used for uniformity correction. The latter can be recognized by observing that the flood-corrected images are markedly less uniform (higher values of IU and rms noise) than the uncorrected images or by looking at the original flood field images if they are available.

A comparison of the IU and rms noise values in Table V shows that the average values are increased slightly when flood correction is applied. This finding may be due to the occasional use of a flood correction that was not current. A

TABLE IX. Precision of contrast measurements for Jaszczak phantom images ($N=7$).

Sphere size (mm)	31.8	25.4	19.1	15.4
Average contrast $\pm 1\sigma$	0.775 ± 0.047	0.567 ± 0.094	0.273 ± 0.056	0.198 ± 0.060
Percent standard deviation	7.95	11.50	21.36	32.28
Range	0.719–0.849	0.409–0.709	0.219–0.358	0.111–0.287

mismatch between the camera uniformity that is present at one point in time and the one that existed when the high-count flood was stored may generate artifacts. The slightly higher value of the IU and/or rms noise may also be a predictable result of the propagation of errors in the renormalization process.

High values of IU and rms noise can also be caused by selecting a filter that retains higher frequencies or has a higher cutoff than those presented in Table II. Low values can be produced by using a smoothing filter and/or a cutoff lower than the Nyquist value. It must be understood that there are significant differences in the actual implementation of what is nominally the *same* filter. Hamming and Shepp-Logan/Hann filters give slightly higher values of reconstructed integral uniformity, rms noise, and contrast, but lower FWHM values. This is in part the explanation for the large range of values shown in Table V as compared to those presented in Table VIII.

Comparison of the contrast measurements presented in Tables VI and VII with those shown in Table IX reveal significant differences. These are also primarily due to variations in reconstruction software but may also reflect differences in energy resolution. For emphasis, the average contrast of the largest sphere for three different models/vendors is presented in Fig. 1, along with the average value for the entire database. Although the sample size for the subsets is small, a significant difference can be appreciated.

In the case of contrast measurements, there is still another factor. Collimators described as ''General Purpose'' by different vendors are not necessarily the same. Some have FWHMs close to what other vendors would call a ''high resolution'' collimator. On the other hand, some ''General Purpose'' collimators are very similar to ''High Sensitivity'' collimators of other manufacturers. Or the collimator resolution may degrade with distance at different rates, depending on the basic design.

It is well known that the system spatial resolution as measured by the FWHM must be one-third to one-half the diameter of a spherical object for quantitative recovery.[18] When this condition is not met, e.g., when a collimator with lower resolution (larger FWHM) is used, there will be a loss of contrast. If the absolute FWHM values in millimeters are reviewed, marked differences are clearly seen. For the general purpose collimators used in this study, the FWHM values ranged from 12.7–19.5 mm at 20 cm in air.

Systems that produce contrast values below the mean minus one standard deviation of those given in Tables VI and VII are probably not operating properly. When larger radii of rotation and/or a low-resolution collimator are used, the contrast values will generally be higher. Apart from any other differences, contrast will also be poorer on systems with poor energy resolution, as previously stated.

If a ''Jaszczak'' or ''Carlson'' phantom is not available, some useful data can be obtained by imaging a cylindrical plastic bottle of approximately 4 l filled with a solution of Tc-99m. This phantom does not enable the user to measure contrast, but integral uniformity and noise can be calculated and proper operation of the attenuation correction software can be verified. The resulting tomographic images can also be evaluated for the presence of ring artifacts. The general statement can also be made that camera stability is more important than superb spatial resolution or uniformity. Uncorrected fluctuations in camera uniformity can produce artifacts which may produce false positive interpretations of clinical studies.

VI. SUMMARY AND CONCLUSIONS

A comprehensive performance testing program is an essential ingredient of high-quality SPECT imaging. This program must include tests of angular uniformity and sensitivity, tomographic spatial resolution, uniformity, and contrast, and the accuracy of attenuation correction. Because the protocol described in this report utilizes standard keyboard commands available on every SPECT system, it is relatively easy to implement. Once a user is familiar with the procedure, the tests can be performed in 2–3 h. Although it is suggested that a system performance test be performed no less than every six months and immediately after service or any change in software or hardware, the actual frequency must be determined by individual system performance. One of the advan-

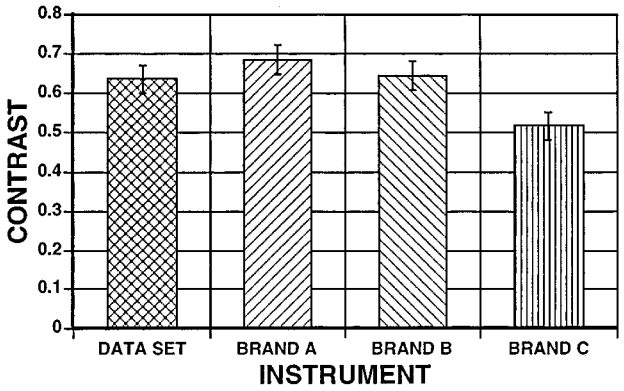

FIG. 1. Contrast for 3.18-cm cold sphere in the Data Spectrum Phantom study for the entire data set and three different subsets. Each subset represents the average calculated contrast for a different model/vendor scintillation camera using a ''Hann'' filter with a 1-Nyquist cutoff. Each subset has at least six instruments.

tages of quantifying SPECT system performance using a phantom is the ability to identify slow deterioration so that repairs can be scheduled at convenient times. However, physicians and technologists should be able to recognize the major types of artifacts that are produced by SPECT systems that are not operating properly.ag

The importance of a comprehensive quality assurance program is clearly stated by Herrera et aZ.:34

"Certainly, the need for careful quality assessment, and thoughtful quality assurance will grow with instrument complexity if new performance capabilities are to be translated into clinical gain."

APPENDIX A

APPENDIX A

SPECT PERFORMANCE TESTS

Date: ___/___/___ Person Performing Test _____

Hospital: _____

_____

_____

City: _____

State:_____ Country: _____

Camera Vendor _____

Model _____

Number of tubes _____

Crystal thickness _____ mm

Computer Vendor _____

Uniformity vs Angle (5M/view-Preset time from 0 degree image)

Al/_____/20% Tc-99m ___ Co-57 ___

0 Deg 5,000,000 cts/ _____ sec
90 Deg _____ cts/_____ sec
180 Deg _____ cts/_____ sec
270 Deg _____ cts/_____ sec
360 Deg _____ cts/_____ sec

Maximum Sensitivity Variation = _____ %

Center-Of-Rotation (Line ____; Off__ On__ axis point)

Activity _____ mCi) Orientation ____
Al/____/____% Date performed ___/___/___
File Name _____ Number of views _____
Time ____ sec Matrix Size 64___ 128___
Cts _____per view Byte___ Word___
Magnification _____ Collimator _____

X Analysis Output:
Mean ____ Max Error _____ Min Error _____
Mean Error _____ Std dev ____
Y Analysis Output:
Mean ____ Max Error _____ Min Error _____
Mean Error _____ Std dev ____

Flood (For Uniformity Correction)

Al/____/____% Date performed _____
File Name _____ Orientation ____
Number of counts _____ Magnification _____
Collimator _____ Matrix Size 64___ 128___
Byte___ Word___
Integral Uniformity in CFOV ____% OPTIONAL
Differential Uniformity in CFOV ___% OPTIONAL
Standard deviation in CFOV _____ OPTIONAL

Resolution Test: Line___ NEMA___ Date Performed _____

Line Source (Activity = _____ mCi)
Al/_____/____%
File Name _____
Number of views _____ Matrix Size 64__ 128__
Magnification _____ Collimator _____
Time/Projection _____ sec Cts/projection _____
Direction: CCW __ CW __ Circular ___ Non Circular ___
Radius of Rotation: Semi-major axis _____ cm
Semi-minor ____ cm Semi-major/Semi-minor = _____
Step/Shoot__ Contin __ Orientation _____
Reconstruction Filter _____ Order ____
Cutoff ___/pix ___/cm or ____ Nyquist
Scale factor _____

Calibration (X direction) (____ pix - ____ pix)/_____ mm
= _____ pix/mm = _____ mm/pixel

Position: Top (File name _____)
FWHM (horizontal) = ____ pix ____ mm
FWHM (vertical) = ____ pix ____ mm

Position: Bottom (File name _____)
FWHM (horizontal) = ____ pix ____ mm
FWHM (vertical) = ____ pix ____ mm

Planar Line:
Distance ____ cm Counts _____
Matrix Size 64 __ 128 ___

Position: Top
FWHM (horizontal) = ____ pix ____ mm

Position: Bottom
FWHM (horizontal) = ____ pix ____ mm

Date Performed _____

Data Spectrum Phantom (Standard ___; Deluxe ___)

Al/_____/____%
Activity ____mCi ____Bq File Name _____
Number of views _____ Matrix Size 64 __ 128 ___
Byte __ Word ___
Magnification _____ Collimator _____
Pixel size (X) _____ mm Pixel size (Y) _____ mm
Time/Projection ____ sec Counts/projection _____
Direction: CCW __ CW __ Circular ___; Non Circular ___
Radius of rotation _____ cm
Step/Shoot __ Contin __ Orientation _____
Reconstruction Filter _____ Order _____
Cutoff ____/pix ____/cm ____Nyquist
Scaling Factor _____
Slices: _____ through _____
Attenuation Coefficient ____/cm or ____/pix

Uniformity and RMS Noise (15 x 15 pix square) - No flood correction

(File name _____) Slice _____
Ring artifacts? Yes___ No___
Mean = ____ cts Standard Deviation ____
Max pixel = _____ cts Min pixel = _____ cts
Integral Uniformity = _____ %
RMS Noise = _____ %

Attenuation correction (no flood correction)

Horiz Profile: Flat __ Flat but tilted (+ or -) __
Over cor'd _____ Under cor'd _____

Vert Profile: Flat __ Flat but tilted (+ or -) __
Over cor'd _____ Under cor'd _____

Contrast (No flood correction)
Slice with spheres ___ Number spheres visualized ___
Ring artifacts? Yes ___ No ___
Spheres (Average counts = _____)

Size (mm)	Minimum pix cts	Contrast
38	_____	_____
31.8	_____	_____
25.4	_____	_____
19.1	_____	_____
15.4	_____	_____

Uniformity and RMS Noise (15 x 15 pix square) - With flood correction

(File name _____) Slice _____
Ring artifacts? Yes___ No___
Mean = ____ cts Standard Deviation ____
Max pixel = _____ cts Min pixel = _____ cts
Integral Uniformity = _____ %
RMS Noise = _____ %

Attenuation correction (With flood correction)

Horiz Profile: Flat __ Flat but tilted (+ or -) __
Over cor'd _____ Under cor'd _____

Vert Profile: Flat __ Flat but tilted (+ or -) __
Over cor'd _____ Under cor'd _____

Slice with spheres ___ Number spheres visualized ___
Ring artifacts? Yes ___ No ___
Spheres (Average counts = _____)

Size (mm)	Minimum pix cts	Contrast
38	_____	_____
31.8	_____	_____
25.4	_____	_____
19.1	_____	_____
15.4	_____	_____

Time required to acquire and process data _____ hrs

[1]J. W. Keyes, Jr., "Perspectives on tomography," J. Nucl. Med. 23, 633-640 (1982).
[2]M. J. Myers and F. Fazio, "The case for emission computed tomography with a rotating camera," Appl. Radiol./NM 10, 127-134 (1981).
[3]D. E. Kuhl and T. P Sanders, "Characterizing. brain lesions with the use of transverse section scanning," Radiology 98, 327-328 (1971).
[4]T. C. Hill, R. D. Lovett, and R. E. Zimmerman, "Quantification of Tc-99 *m* -glucoheptonate in brain lesions with single-photon ECT," in *Single Photon Emission Computed Tomography and other Selected Computer Topics,* edited by R. R. Price, G. L. Gilday, and B. Y. Croft (Society of Nuclear Medicine, New York, 1980), pp. 169-176.
[5]D. E. Kuhl, J. R. Barrio, S. C. Huang, C. Selin, R. F. Ackermann, J. L. Lear, J. L. Wu, T. H. Lin, and M. E. Phelps, "Quantifying local cerebral blood flow by N-isopropyl-p[I-123]iodoamphetamine (IMP)," J. Nucl. Med. 23, 196-203 (1982).
[6]R. J. Jaszczak, E R. Whitehead, C. B. Lim, and R. E. Coleman, "Lesion detection with single-photon emission computed tomography (SPECT) compared with conventional imaging," J. Nucl. Med. 23, 97-102 (1982).
[7]P. H. Murphy, "Acceptance testing and quality control of gamma cameras, including SPECT," J. Nucl. Med. 28, 1221-1227 (1987).
"R. J. English and S. E. Brown, SPECT Single-Photon Emission Computed Tomography: A Primer (The Society of Nuclear Medicine, New York, 1986).
[9]*PublicationlNo. NUI (NEMA NU I-1986)* (National Electrical Manufacturers Association, Washington, DC, 1986).
[10]*Rotating Scintillation Camera SPECT Acceptance Testing and Quality Control, AAPM Report No. 22* (Published for the American Association of Physicists in Medicine by the American Institute of Physics, New York, 1987).
[11]C. I. Coleman, "Effects of perturbing magnetic fields on the performance of photoelectronic sensors," Rev. Sci. Instrum. 53, 735 (1982).
[12]F. Takasaki, K. Ogawa, and K. Tobimatsu, "Performance of a photomultiplier tube with transmissive dynodes in a high magnetic field," Nucl. Instrum. Meth. 228, 369 (1985).
[13]W. L Rogers, H. N. Clinthorne, B. A. Harkness, K. F. Koral. and J. W. Keyes, Jr., "Flood-field requirements for emission computed tomography with an Anger camera," J. Nucl. Med. 23, 162-168 (1982).
[14]S. Larsson and A. Israelsson, "Considerations on system design, implementation and computer processing in SPECT," IEEE Trans. Nucl. Sci. NS-29. 1331 (1982).
[15]J. Bieszk, "Performance changes of an Anger Camera in magnetic fields up to 10 G," J. Nucl. Med. 27. 1902-1907 (1986).
[16]A. E. Todd-Pokropek and P. H. Jarritt, in *Computed Emission Tomography,* edited by P. J. Ell and B. L. Holman (Oxford University, New York, 1982). pp. 374-375.
[17]T. K. Johnson, D. L. Kirch. B. H. Hasegawa, D. Thompson, and P. P. Steel, "Spatial/temporal/energy dependency of scintillation camera nonlinearities," in *Emission Computed Tomography: Current Trends,* edited by P. D. Esser (The Society of Nuclear Medicine, New York. 1983).
[18]E. Hoffman S. C. Huang, and M. E. Phelps, "Quantitation in positron emission computed tomography: 1. Effect of object size," J. Comput. Assist. Tomogr. 3, 299-308 (1979).
[19]L. T. Kircos, J. E. Carey, Jr, and J. W. Keyes, Jr., "Quantitative organ visualization using SPECT," J. Nucl. Med. 28, 334-341 (1987).
[20]F. Soussaline, A. E. Todd-Pokropek, and C. Raynaud, "Quantitative studies with the gamma camera: Correction for spatial and energy distortion," in Review of Information Processing of Medical Imaging, edited by A. B. Brill and R. R. Price (Oak Ridge National Lab, Oak Ridge, TN, 1977), pp. 360-375.
[21]A. E. Todd-Pokropek, F. Erbsmann, and E Soussaline, "The nonuniformity of imaging devices and their impact in quantitative studies," in Medical Radionuclide Imaging, Vol. I (International Atomic Energy Agency, Vienna, 1977), pp. 67-82.
[22]R. Wicks and M. Blau, "Effect of spatial distortion on Anger camera field uniformity correction," J. Nucl Med. 20, 252-254 (1979).
[23]L. Shabason, D. Kirch, M. LeFree, and W. Hendee, "Online digital methods for correction of spatial and energy dependent distortion of Anger camera images," in Review of Information Processing of Medical Imaging, edited by A. B. Brill and R. R. Price (Oak Ridge National Lab, Oak Ridge, TN, 1977), pp. 376-388.
[24]G. T. Gullberg, "An analytical approach to quantify uniformity artifacts for circular and noncircular detector motion in single photon emission computed tomography imaging," Med. Phys. 14, 105 (1987).
[25]A. Todd-Pokropek, S. Zerowski, and F. Soussaline, "Non-uniformity and artifact creation in emission tomography," J. Nucl. Med. 21, P38 (1981) (abstr.).
[26]A. van Aswegen, P. H. Pretorius, C. P. Herbst, M. G. Lotter, and P. C. Minnaar, "The effect of different flood field correction methods on reconstructed SPECT images," Phys. Med. Biol. 34, 633-635 (1989).
[27]K, L. Greer R. E. Coleman, and R. J. Jaszczak, "SPECT: A practical guide for users," J. Nucl. Med. Tech. 11, 61-65 (1983).
[28]J. R. Halama and R. E. Henkin, "Quality assurance in SPECT imaging," Appl. Radiol., 41-50 (May 1987).
[29]K. D. Brust and M. M. Graham, "Aspects of patient imaging with SPECT," J. Nucl. Med. Tech. 15, 133-137 (1987).
[30]C. R. Appledorn, B. E. Oppenheim, and H. N. Wellman, "Performance measures in the selection of reconstruction filters for SPECT imaging," J. Nucl. Med. 26, P35 (1985).
[31]B. A. Harkness, W. L. Rogers, H. N. Clinthome, and J. W. Keyes, Jr., "SPECT: Quality control procedures and artifact identifications," J. Nucl. Med. Tech. 11, 55-60 (1983).
[32]R. J. Jaszczak, P. H. Murphy, D. Huard, and J. A. Burdine, "Radionuclide emission computed tomography of the head with Tc-99m and a scintillation camera," J. Nucl. Med. 18, 373-380 (1977).
[33]A. C. Kac and M. Slaney, Principles of Computed Tomographic Imaging (IEEE, New York, 1988).
[34]N. E. Herrera, in Medical Radionuclide Imaging, Vol. II (International Atomic Energy Agency, Vienna, 1981), pp. 177-187.